

# Predicting the Emergence of Induction Heads in Language Model Pretraining

Tatsuya Aoyama<sup>1</sup> Ethan Gotlieb Wilcox<sup>1</sup> Nathan Schneider<sup>1</sup>

## Abstract

Specialized attention heads dubbed *induction heads* (IHs) have been argued to underlie the remarkable in-context learning capabilities of modern language models; yet, a precise characterization of their emergence, especially in the context of language modeling, remains wanting. In this study, we investigate the relationship between statistical properties of the training data and IH formation in both natural and synthetic training data settings. We show that: (1) A simple equation combining batch size and context size predicts the point at which IHs form and that this emergence point is agnostic to model size; (2) Surface bigram repetition frequency and reliability strongly affect the formation of IHs, and we find an effective Pareto frontier in terms of these two values; (3) local dependency with high bigram repetition frequency and reliability is sufficient for IH formation, but when the frequency and reliability are low, categoriality and the shape of the marginal distribution matter.

## 1. Introduction

The practical utility of modern large language models (LLMs) depends heavily on their ability to perform in-context learning (ICL), broadly construed as performing a task based on the input provided at inference time. Various accounts have been provided to explain the internal workings of this capability, and among them are studies that find certain attention heads affecting language models (LMs)’ ICL capabilities (Olsson et al., 2022; Edelman et al., 2024; Reddy, 2024; Yin & Steinhardt, 2025). Olsson et al. (2022) maintain that specialized heads that emerge abruptly during pretraining, dubbed *induction heads*, are primarily responsible for the emergent ICL capabilities LMs exhibit. Edelman et al. (2024) mathematically show the ICL

<sup>1</sup>Department of Linguistics, Georgetown University. Correspondence to: Tatsuya Aoyama <ta571@georgetown.edu>.

is equivalent to a type of Bayesian inference, and that induction heads are indispensable in making this inference. The emergence of such heads during pretraining is sometimes referred to as phase change or phase transition (Chen et al., 2024; Aoyama & Wilcox, 2025). A broader phenomenon of phase transition is not limited to the text modality, and has been observed in vision models (Okawa et al., 2023; Park et al., 2024).

It has been shown that induction heads form in LMs very early in pretraining, regardless of the model size, as long as the model has multiple heads and at least 2 layers (Olsson et al., 2022). While the behavior and mechanism of induction heads are relatively well-understood (Elhage et al., 2021; Olsson et al., 2022; Edelman et al., 2024), it is not clear *when* and *why* such heads form naturally when trained on language data. In other words, we ask: when exactly do induction heads emerge in LMs, and what properties of natural language give rise to induction heads (IHs) formation, potentially by incentivizing the copying behavior in transformer LMs?

In this study, through a series of experiments using both natural and synthetic data, we draw the following conclusions: (1) A simple equation combining batch size and context size can predict the point at which induction heads form (Section 5). (2) The surface bigram repetition frequency and reliability strongly affect the formation of induction heads, and a Pareto frontier can be described in terms of these two values (Section 6). (3) Local dependency, high frequency and reliability are sufficient for induction head formation, but when the frequency and reliability are low, the presence of categoriality in the data-generating process, and the shape of the marginal distribution matter (Section 7).<sup>12</sup>

## 2. Relevant Work

Factors that affect phase transition, particularly the formation of induction heads, are not fully understood. Induction

<sup>1</sup>Code available at <https://github.com/t-aoyam/predict-ih-review/>.

<sup>2</sup>We will use emergence, phase change, and phase transition interchangeably in this paper.

heads are often associated with LMs’ ICL capabilities.<sup>3</sup> Chan et al. (2022) study the data properties that lead to different learning outcomes in a few-shot learning of image classification, where few-shot examples are image-label pairs. They find that (1) burstiness (similar things appearing in clusters), (2) within-class variation, and (3) dynamic class membership all promote ICL and demote in-weight learning (IWL). Interestingly, making the marginal distribution of the labels Zipfian was the only variable that led to high ICL and IWL simultaneously.

Edelman et al. (2024) proposes a synthetic task dubbed ICL Markov Chain (ICL-MC) using a Markov Process involving 2-8 symbols. Taking a Bayesian approach to ICL (Xie et al., 2022), Edelman et al. (2024) randomly initialize the transition matrix at the beginning of each epoch, thereby making it impossible to learn the underlying distribution of the symbols. They find that the models sequentially go through phases where their predictions most closely match the uniform distribution, then in-context unigram counts, and lastly in-context bigram counts. They show that by forming induction heads that attend to all of the bigram continuations of the current token in the preceding context, models achieve the Bayes-optimal bigram solution.

ICL is often studied as a few-shot learning (e.g., Chan et al., 2022; Singh et al., 2024) with input-label (e.g., image-label) pairs, or with a synthetic setting that necessitates ICL as opposed to IWL (e.g., Edelman et al., 2024; Park et al., 2025). Park et al. (2025) propose a novel synthetic sequence modeling task using a mixture of Markov chains; however, in LM pretraining, it is unlikely that each batch comes from a completely different distribution of tokens. As such, it is yet to be clear why LMs, which are trained on natural language through next token prediction, form induction heads (and ICL capabilities), and what properties of natural language promote such learning dynamics. Furthermore, the point at which induction head formation occurs is not fully understood. Some report a narrow range (1B–3B pretraining tokens; e.g., Olsson et al., 2022) while others find a much wider range (64M–2B pretraining tokens; Aoyama & Wilcox, 2025). Zucchet et al. (2025) is a rare exception that studies the emergence point; however, they focus on a general framework called sparse attention using a synthetic associative recall task. We focus specifically on the emergence of induction heads in the naturalistic language modeling task.

To fill these gaps, in this study, we aim to find (1) the point at which induction heads emerge, and (2) precise data properties that promote the formation of induction heads.

<sup>3</sup>Olsson et al. (2022) claim that induction heads are primarily responsible for ICL, whereas Yin & Steinhardt (2025) find that a different set of heads, dubbed *function vector heads*, are performing few-shot-learning-style ICL.

### 3. Methods

#### 3.1. Metrics

IHs are defined by the copying behavior, such that if the model has seen an  $\langle A, B \rangle$  sequence *in-context* and the current token is A, then an IH is a head that promotes the prediction of B as the next token, completing the  $\langle A, B, \dots, A, B \rangle$  sequence.

**Prefix-matching Score.** Following Olsson et al. (2022), we quantify this behavior using prefix-matching score (PS). Given a random sequence of tokens  $\mathbf{x}$  repeated twice, PS of a head  $h$  at layer  $l$  is its average attention from the source token  $x_i$  to the next token of its previous occurrence:

$$\frac{1}{|\mathbf{x}| - 1} \sum_{i=|\mathbf{x}|+1}^{2|\mathbf{x}|} \alpha^{(h,l)}(x_i, x_{i-(|\mathbf{x}|-1)}) \quad (1)$$

As to the size of the sequence  $\mathbf{x}$ , TransformerLens library (Nanda & Bloom, 2022) adopts  $|\mathbf{x}| = 50$ , which we also do; however, when analyzing models with smaller context sizes, we adjust  $|\mathbf{x}|$  accordingly:  $|\mathbf{x}| = \min(\frac{|\text{context}|}{2}, 50)$ .

**Logit Attribution.** Similarly, Olsson et al. (2022) define a metric called logit attribution (LA). As opposed to PS, which measures a given head’s attention to the token of interest, LA measures the actual contribution of a given head’s output to the model’s final logit of the token of interest via the residual stream. The raw logit contribution  $C \in \mathbb{R}^{|\mathcal{V}|}$  of an output  $x^{h,l}$  from a given head  $h$  at layer  $l$  is computed by passing it through the linear layer of the attention block  $W_O$  and the final unembedding layer  $U$ :

$$(x^{h,l} W_O) U \quad (2)$$

Following Olsson et al. (2022), we then center and normalize the positive logit contribution to all tokens in the test sequence  $\mathbf{x}$  and compute the ratio of the logit contribution to the target token to the rest of the tokens in the sample. Note that since all models used in this study (GPT2, Pythia) employ pre-layer normalization, there exists a direct path from a given head’s output to the final logit calculation. LA captures each head’s contribution through this path. However, it is important to note that the rest of the contribution (e.g., a head’s contribution through subsequent layers) is not captured in LA.

**Associative Recall.** Lastly, we also measure how often a model predicts B when given  $\langle A, B, \dots, A \rangle$ , a metric referred to as associative recall (AR). It can be measured by accuracy:

$$\frac{1}{|\mathbf{x}| - 1} \sum_{i=|\mathbf{x}|+1}^{2|\mathbf{x}|} \mathbb{1}\{f(\mathbf{x}_{<i}) = x_i\} \quad (3)$$

and by the mean rank of the target token B:

$$\frac{1}{|\mathbf{x}| - 1} \sum_{i=|\mathbf{x}|+1}^{2|\mathbf{x}|} \text{rank}(x_i; f(\mathbf{x}_{<i})) \quad (4)$$

As opposed to the previous two metrics, which are head-level, these metrics are model-level. As reported later, the abrupt improvement in AR always follows that in PS and LA, in line with the findings from Reddy (2024). Also, given a high correlation between PS and LA, we report the analyses of PS in the main body of this paper.

### 3.2. Models and Checkpoints

At least 2 attention layers have been shown to be necessary for the model to perform the induction task (Olsson et al., 2022; Reddy, 2024; Ekbote et al., 2025) unless the model’s hidden dimension is increased exponentially (Sanford et al., 2024). In fact, models with 2 layers have recently been shown to be sufficient to approximate any-order Markov chain (Ekbote et al., 2025). Given these findings, we use a 50M-parameter GPT2 (Radford et al., 2019) with 2 layers and 8 attention heads per layer with the hidden dimension of 768 for all experiments. For the first experiment (Section 5), to study the effect of model size, we also train larger models with 125M parameters and 350M parameters and include models up to 7B parameters for inference. See Appendix A for the details on model architecture and training setup.

For experiments with natural language (Section 5), we adopt a pretrained GPT2 tokenizer with a vocabulary size of 50,257, unless otherwise specified. All models analyzed in this study were trained from scratch for 1B pretraining tokens. We save intermediate checkpoints at 250K and 500K tokens, [1M, 10M] tokens at 1M increments, [10M, 100M] tokens at 10M increments, and [100M, 1B] tokens at 100M increments, resulting in 30 checkpoints per model. We additionally use pretrained Pythia models (Biderman et al., 2023) for a follow-up analysis (e.g., Figure 3). Note that, Pythia models were deemed the only available model family with early enough checkpoints available to study the emergence of induction heads, which is known to happen very early in pretraining (64M-3B pretraining tokens; Olsson et al., 2022; Aoyama & Wilcox, 2025). For example, OLMo models provide checkpoints for every 1000 steps of pretraining (Groeneveld et al., 2024), meaning that the earliest model checkpoint is already trained on 4B tokens, likely after the phase transition of interest.

For experiments with synthetic language (Sections 6 and 7), we adopt a vocabulary size of 10,000. We do not use a tokenizer as we only work with token IDs. Note that the change in vocabulary size will likely affect the emergence points (Singh et al., 2024; Zucchetti et al., 2025); however, this shouldn’t change the results of our analyses in these

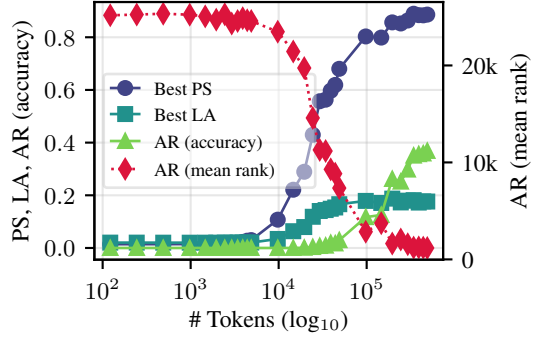


Figure 1. Developmental trajectories of PS, LA, AR accuracy, and AR mean rank. The first three metrics are plotted in the scale on the left  $y$ -axis, and the last metric in the scale on the right  $y$ -axis.

experiments, as we only focus on *whether* IHs emerge or not, and not on *when* they do, in Section 6 and Section 7.

### 3.3. Data

For natural texts (Section 5), unless otherwise specified, we use the English subcorpus from the Common Crawl Corpus (CC100; Conneau et al., 2020; Wenzek et al., 2020). We create a sample of 1B tokens from this corpus, using the pretrained GPT2 tokenizer. As mentioned earlier, all models are trained for 1 epoch on this sample, for the total of 1B tokens. For semi-natural data (Section 6) and synthetic data (Section 7), we use a token-to-token transition matrix, and the details are provided in each section.

## 4. Metric Selection

Before diving into the main experiments, as briefly mentioned earlier, we show how PS, LA, and AR develop during pretraining. Figure 1 shows a sample model (GPT2 125M) trained with batch size of 16 and context size of 128. Clearly, all four metrics go through an abrupt change at around the same time. Notably, AR accuracy seems to increase slightly later compared to the other three metrics. It is important to recall that the best PS and best LA are head-level change in the strategy a model is employing, and that AR (mean rank) measures model’s change in the direction of predicting the target token B, even when it is not the most probable token. On the other hand, AR (accuracy) only improves when the target token B is the most probable token; in other words, the model’s improvement from ranking the token B as the least probable (rank 50,257) to second most probable (rank 2) is not captured in this metric. Given these observations, for simplicity and readability, we only report PS in the main body of this paper, while replicating similar analyses with other metrics in Appendix J.

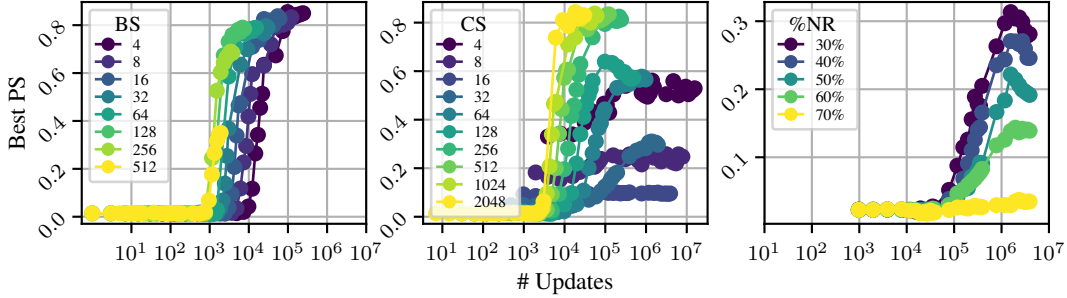


Figure 2. Developmental trajectories of PS of LMs with various batch sizes (left), context sizes (center), and repetitions (right) over the course of 1B tokens of pretraining, plotted against the number of updates (a) and the number of tokens (b). BS, CS, %NR stands for batch size, context size, and the proportion of chunks with no repetitions, respectively.

## 5. Experiment 1: Natural Data

### 5.1. Methods

As briefly introduced earlier, Aoyama & Wilcox (2025) find that training an LM with different batch sizes results in different phase transition points. In this experiment, we change context size and batch size to investigate their effect on the formation of IHs. Specifically, we experiment with log-spaced batch and context sizes of  $\{4, 8, 16, 32, 64, 128, 256, 512\}$ , and  $\{4, 8, 16, 32, 64, 128, 256, 512, 1024, 2048\}$ , respectively. Since grid search is expensive, we fix the batch size at 16 while changing the context size, and fix the context size at 1024 while changing the batch size. We additionally test the effect of bigram repetitions alone by selecting subsets of the pretraining data and manipulating the proportion of bigram repetitions.

### 5.2. Results

**Batch Size.** In Figure 2 (left), we find (1) the larger the batch size, the lower the eventual PS; in other words, a larger batch size leads to weaker IHs at the end of the pretraining, and (2) the smaller the batch size, the later the “spike” in PS; in other words, training an LM with a smaller batch size results in later emergence of IHs, as measured by the number of updates.

**Context Size.** In Figure 2 (center), we find that (1) the smaller the context size, the later the elbow of the curve is, meaning that the onset of the IH formation is later in pretraining, as measured by the number of updates, and (2) the smaller the context size, the flatter the slope once IHs start forming, and the extreme case (context size  $\leq 16$ ) is a flat line, or the complete suppression of IHs (see Appendix B on how we determine “random” attention). For the shifting effect in (1), since this effect was observed both when changing batch size and context size, we suspect that this could be attributed to the number of tokens the model

is exposed to at each update. For the slanting effect in (2), we suspect that, in natural texts, a larger context size will naturally contain more occurrences of  $\langle A, B, \dots, A, B \rangle$  patterns, which may have a threshold below which IHs will not form.

It is important to note that we observe an inverse shifting effect when plotting against the number of pretraining *tokens* in Figure 6 in Appendix C, thereby ruling out the possibility that the observed shifting effect is an artifact of each point on *x*-axis representing a different number of pretraining *tokens*.

**Repetition.** The number of bigram repetitions increases as context size grows (see Figure 7 in Appendix E), which we hypothesize to cause the slanting effect of the context size. To tease apart these two phenomena, we manipulate the occurrence rate of bigram repetitions within each chunk, while controlling for the batch size and context size. See Appendix E for more details on how we manipulate the repetition rate while controlling for the context size. In Figure 2 (right), the lower the proportion of chunks with no bigram repetitions, the higher the best PS a given model achieves. Second, there is no “shifting” of the curve, and we only observe the “slanting” effect. This confirms the observation earlier that the “shifting” is due to the number of tokens an LM sees per update, and “slanting” is due to the rate at which an LM encounters repeated bigrams.

**Predictive law.** We have seen that context size and batch size affect the phase transition point. Here, we ask: can we predict the phase transition point only using the training configuration as variables (i.e., before we train the model)? In existing studies, points at which a phenomenon of interest happens are often defined in terms of the number of pretraining tokens (e.g., Olsson et al., 2022; Oh & Schuler, 2023), or in floating-point operations (FLOPs; e.g., Kaplan et al., 2020). It has been shown that LMs seem to go through a phase transition at different points in terms of the number of pretraining tokens (Aoyama & Wilcox, 2025) and the

number of updates (Figure 2), and hence it is not a good candidate to describe the phase transition point. We can also infer that FLOPs is not a reliable measure to capture this either, because (1) FLOPs is a function of input and model size, and (2) models that are orders of magnitude different in size seem to go through a phase transition at around the same time in terms of the number of pretraining tokens (e.g., Olsson et al., 2022). Nonetheless, we start with a full regression model that takes into account the effect of batch size, context size, and model size:

$$U_{\text{PT}} = e^{\alpha} B^{\beta} C^{\gamma} P^{\theta} \quad (5)$$

where  $U_{\text{PT}}$  is the number of updates at which a given model goes through phase transition (as defined in Section D.1).  $B, C, P, \beta, \gamma, \theta$  represent batch size, context size, and the model size as measured in the number of parameters, and their corresponding coefficients, respectively.  $e^{\alpha}$  serves as an intercept, as we will see below. Once a regression is fit in log-space with a total of 35 models (see Section D.2 for the details of these models),  $\theta$  turns out to be the only *non*-significant coefficient. We provide the details of these test statistics in Section D.3, and proceed with a regression model without model size.

As such, we propose a simple model-size-agnostic law that predicts the number of updates at which a given LM goes through the phase transition based on the context size and batch size alone:

$$U_{\text{PT}} = e^{\alpha} B^{\beta} C^{\gamma} \quad (6)$$

Following Kaplan et al. (2020), we estimate the parameters  $\alpha, \beta$ , and  $\gamma$  using a simple ordinary least squares regression in log space:

$$\log U_{\text{PT}} = \alpha + \beta \log B + \gamma \log C \quad (7)$$

Fitting this model, we obtain  $\alpha = 13.26$ ,  $\beta = -0.37$ , and  $\gamma = -0.62$  (see Table 4 for all test statistics). Calling  $e^{\alpha} = 750000$  a constant  $T$  and plugging these parameters back into Equation (6), we obtain:

$$U_{\text{PT}} = \frac{T}{B^{0.37} C^{0.62}} \quad (8)$$

$$T = U_{\text{PT}} B^{0.37} C^{0.62}$$

The key intuition behind Equation (8) is that the model-agnostic constant  $T$  is a function of the *quantity* of training, or the number of updates  $U_{\text{PT}}$ , at which phase transition occurs. At the same time, the *quality* of each update matters, and it correlates with the number of tokens the model sees at each update, which is a function of context and batch sizes  $B^{0.37} C^{0.62}$ . Let us call the generalized form of the right hand side (RHS) of this equation,  $U B^{0.37} C^{0.62}$ , the number of token-weighted updates (TWUs), given that it

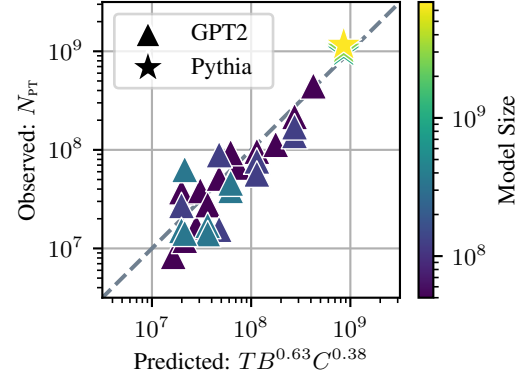


Figure 3. Predicted and observed number of pretraining tokens at which phase transition occurs.  $x$ -axis and  $y$ -axis represent predicted and observed points of phase transition, expressed in the number of pretraining tokens, respectively. A strong correlation of  $r = .98$  ( $p < .001$ ) is found.

is the number of updates scaled by batch size and context size to incorporate the number of tokens seen at each update. Equation (8) suggests that the number of TWUs at which phase transition occurs can be expressed as a constant  $T$  across model and training configurations.

To further verify that this simple law indeed predicts the phase transition point of LMs trained with various training configurations, we can reformulate Equation (8) to predict the number of tokens  $N$ :

$$T = U_{\text{PT}} B^{0.37} C^{0.62} \quad (9)$$

$$TB^{0.63} C^{0.38} = U_{\text{PT}} BC$$

Because  $N = UBC$  by definition, RHS is  $N$ , and we get:

$$N_{\text{PT}} = TB^{0.63} C^{0.38} \quad (10)$$

The left hand side (LHS) of Equation (9) is the *observed* number of pretraining tokens at which phase transition occurs, and the RHS is the *predicted* point based on context size  $C$  and batch size  $B$ , as well as the empirically found constant  $T = e^{13.26}$ . Now we can predict the number of tokens  $N$  at which phase transition occurs, based on a constant  $T$  and training configurations  $C$  and  $B$ . In Figure 3,  $x$ -axis and  $y$ -axis correspond to the LHS and RHS, or the predicted and observed number of pretraining tokens at which phase transition occurs, respectively. We can see a strong correlation of  $r > .99$  before the log-transformation (for readability, as shown in Figure 3), and  $r = .98$  after the log-transformation, where  $p < .001$  for both. This law holds for more than 3 orders of magnitude in model size (50M–7B), and 5 orders of magnitude in the number of tokens per update (500–2M).

## 6. Experiment 2: Semi-Natural Data Using Natural Bigram Statistics

### 6.1. Methods

In Figure 2 (right), we manipulated the repetition rate at the chunk level; in other words, we only manipulated the proportion of chunks with at least one bigram repetition. This repetitiveness at the chunk level is coined *burstiness* as a discrete variable in Chan et al. (2022) and extended to a continuous variable in Reddy (2024) for an in-context classification task. Zucchetti et al. (2025) also reports the effect of repetition in training data; however, this is again at the sequence level and on associative recall task, as opposed to language modeling task. To more precisely manipulate the repetition rate at the token level and in the context of language modeling, we define two metrics, *frequency* and *reliability* of repetition.

*Frequency* measures the relative frequency at which  $\langle A, B, \dots, A \rangle$  is observed in a given data, expressed as  $P(A, B, \dots, A)$ . It is simply the proportion of tokens in a given data that complete a  $\langle A, B, \dots, A \rangle$  sequence as the second occurrence of A, where  $A \neq B$ .

*Reliability* measures the conditional probability with which B is observed given  $\langle A, B, \dots, A \rangle$ , expressed as  $P(B | A, B, \dots, A)$ . It is the proportion of tokens in a given data that complete a  $\langle A, B, \dots, A, B \rangle$  sequence as the second occurrence of B, where  $A \neq B$ , divided by the aforementioned *frequency*. See Appendix F for a detailed walk-through of these two metrics, and Figure 8 for how these two metrics change for various context sizes in natural data.

To create training data that resemble natural data and also satisfy desired values for these two metrics, we first generate a token-to-token transition matrix based on the bigram statistics from natural data, CC100. We then sample from this matrix, while imposing the specified frequency-reliability configuration, and train an LM for each configuration. See Appendix G for more details on the sampling procedure. We also note that, due to the sampling procedure, the two properties are imposed on the second half of the sequence, rather than the entire sequence.

### 6.2. Results

Each cell of Figure 4 represents an LM trained in the configuration specified by the  $x$  and  $y$  axes. We conduct a grid search over a search space defined by all possible combinations of each metric ranging from  $\{0.1, 0.3, 0.5, 0.7, 0.8\}$ . We initially found that the formation of PS was insensitive to different values of  $P(B | A, B, \dots, A)$  when  $P(A, B, \dots, A) \geq 0.1$ , and hence conducted an additional grid search over  $P(A, B, \dots, A) \in \{0.01, 0.03, 0.05, 0.07, 0.09\}$ . With the total of 50 mod-

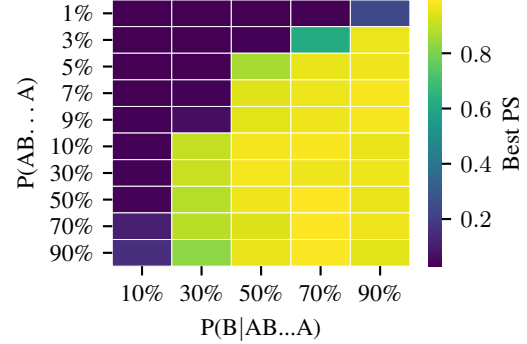


Figure 4. Best PS across all heads at the end of the training for each frequency-reliability combination. Scores are represented in colors, with brighter colors representing higher scores.

els colored based on the best PS in Figure 4, we can clearly see a Pareto frontier, where a decrease in either value will result in the failure of IH emergence. Notably, LMs studied here seem to show stronger sensitivity to reliability than to frequency. In the bottom half of Figure 4,  $[i, j]$  and  $[j, i]$  do not always show the same result. For example, the 10% row always forms IHs except for the 10% column; however, no LMs under the 10% column form an IH. This is notable, given that  $[i, j]$  and  $[j, i]$  cells have identical numbers of bigram repetitions because  $P(A, B, \dots, A, B) = P(B | A, B, \dots, A)P(A, B, \dots, A)$ .

## 7. Experiment 3: Synthetic Data

The previous experiment relied on a Markov Process obtained from a naturally occurring text (i.e., CC100). The main goal of this last experiment is to describe the properties of the underlying Markov Process necessary and/or sufficient for IH formation.

### 7.1. Methods

For simplicity, and to allow for a more precise control over the data properties, we limit our scope to the second order Markov Process as the underlying generative process, which can be expressed as a token-to-token transition matrix  $T \in \mathbb{R}^{|\mathcal{V}| \times |\mathcal{V}|}$ . Once the desired properties (see below) are specified, we optimize the matrix using the Adam optimizer (see Appendix H for details).

We consider three properties that we hypothesize to affect the formation of IHs: (1) local dependency, (2) categoriality, and (3) the shape of the marginal distribution. For (1) local dependency ( $\pm D$ ), it is construed as:  $+D$  iff  $P(w_{t+1} | w_t) \neq P(w_{t+1})$ . In other words, unless the random variable  $W$  is i.i.d. at each position  $t$ , we consider this variable as  $+D$ . This simply means that a distribution is  $+D$  if a word affects what word comes next.

Table 1. Markov Processes used for pretraining data generation in Experiment 3. Each row represents a matrix that defines the Markov Process. The **Properties** column lists desired properties the matrix was optimized for, and the **Statistics** column summarizes the actual statistical properties each matrix had at the end of the optimization process. LD and CAT represents the binary variables local dependency and categoriality, respectively. H measures the entropy of the data, and KL divergence measures the fit between the desired distribution (as shown in the **Properties** column) and the actual marginal distribution of the generated matrix.

	Properties			Statistics			
	Marginal	LD	CAT	H( $\cdot$ )	Intra-group	Inter-group	$D_{KL}(\cdot \parallel \text{target})$
Zipf <sub>[+D+C]</sub>		✓	✓	6.2142	0.3987	0.1007	0.0001
Zipf <sub>[+D-C]</sub>	Zipfian	✓	✗	6.1988	0.0999	0.1010	0.0001
Zipf <sub>[-D-C]</sub>		✗	✗	9.5239	-	-	-
Unif <sub>[+D+C]</sub>		✓	✓	6.5388	0.3719	0.0010	4e-6
Unif <sub>[+D-C]</sub>	Uniform	✓	✗	6.4759	0.0873	0.0104	0.0001
Unif <sub>[-D-C]</sub>		✗	✗	13.2734	-	-	-
Gaus <sub>[+D+C]</sub>		✓	✓	6.2435	0.3995	0.1003	0.0001
Gaus <sub>[+D-C]</sub>	Gaussian	✓	✗	6.2407	0.0999	0.1002	0.0001
Gaus <sub>[-D-C]</sub>		✗	✗	12.3490	-	-	-

For (2) categoriality ( $\pm C$ ), as IHs have been shown to copy abstract patterns, such as semantic categories (e.g., color-object sequences; Olsson et al., 2022), we suspect that the presence of categories promotes the formation of IHs. To make this property compatible with the optimization process, we define categoriality by inter-group and within-group similarity scores. We define the presence ( $+C$ ) and absence ( $-C$ ) of categoriality as having within-category similarity of 0.4 and 0.1, respectively. Between-category similarity was always set to 0.1. We first assign  $\frac{|\mathcal{V}|}{|\mathcal{C}|}$  tokens into each category  $c \in \mathcal{C}$ , thereby creating  $|\mathcal{C}|$  groups with disjoint members. We then define inter-group similarity as the average cosine similarity between words (i.e., each of the  $|\mathcal{V}|$  rows of the transition matrix  $\mathcal{T} \in \mathbb{R}^{|\mathcal{V}| \times |\mathcal{V}|}$ ) from a given category  $c$  and words from a different category  $c'$ :

$$\frac{1}{N} \sum_{c, c' \in \mathcal{C}, c \neq c'} \sum_{w \in c} \sum_{w' \in c'} \text{sim}(w, w') \quad (11)$$

where  $N$  is the number of such word pairs. Within-category similarity is likewise defined as the average similarity between all pairs of words that belong to the same category. If a distribution has a high within-category similarity but a lower across-category similarity, it means that categories exist in this distribution.

Lastly, for (3) marginal token distribution shape, we consider 3 distribution shapes that are increasingly less uniform: Uniform, Gaussian, and Zipfian distributions. This is because natural language is uniquely characterized by a Zipfian distribution, an inverse power law that expresses the frequency of a given word as inversely correlated with its rank, and that it has been shown to affect the emergence of ICL capabilities (e.g., Chan et al., 2022).

Taken together, we have  $3$  (shape of marginal distribution)  $\times 2$  (local dependency)  $\times 2$  (categoriality) = 12 unique data configurations. We note that a subset of these configurations, specifically the  $-D+C$  configurations, are not conceivable. This is because, since  $-D$  is defined as a matrix with identical rows (each token’s transition distribution is identical), both within-category and between-category similarities are 1. Hence, we have the total of 9 combinations of features, each of which is a process that generates the pretraining data.

Table 1 summarizes the properties as well as the actual statistics of each of these distributions.  $H(\cdot)$  measures the conditional entropy of the distribution, estimated by taking the sum of the entropies of each row  $\mathbf{r} \in \mathbb{R}^{|\mathcal{V}|}$ , weighted by the stationary distribution (see Appendix I). Note that the last row of each block, marked by the  $-D$  configuration, has a higher entropy. This is because, for the  $-D$  configuration, each row of the matrix is identical to each other, and each word in this distribution is i.i.d. Hence, once the shape of the marginal distribution is specified, the entropy of this matrix is automatically determined. For example,  $\text{Unif}_{[-D-C]}$  is by definition the maximally entropic distribution over  $|\mathcal{V}|$  items:  $\log_2 |\mathcal{V}|$ .  $D_{KL}(\cdot \parallel \text{target})$  is the KL divergence between the desired marginal distribution and the actual marginal distribution of the generated matrix. We can see that the divergence is very small for all distributions. Intra-group similarities, inter-group similarities, and  $D_{KL}(\cdot \parallel \text{target})$  for the  $\text{Dist}_{[-D-C]}$  configs are 1, 1, 0, respectively, by definition.

## 7.2. Results

In Figure 5, we first find that no property is by itself a *sufficient* condition for IH formation. For example, the highest bigram repetition condition (column under 0.9-0.9) still fails

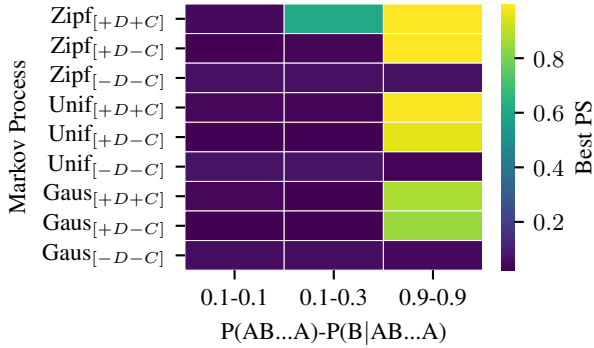


Figure 5. Induction head formation, as measured by PS, in each of the pretraining data generated by the Markov Processes. Each column represents a frequency-reliability configuration.

to produce IHs under the  $-D$  condition. Second, related to the first point, local dependency is a *necessary* condition; no configurations with  $-D$  form IHs. Intuitively, if each token is i.i.d., the model might not be learning to utilize past tokens in context to facilitate the next token prediction. Third, as we showed in Section 6, we reconfirm that some level of bigram repetition is a *necessary* condition (Section 6). No configurations under the 0.1-0.1 column promote the formation of IHs.<sup>4</sup> Lastly, interestingly, marginal distribution and categoriality seem to matter only when the bigram repetition is near the Pareto frontier. Whereas  $\pm C$  and distribution shape do not affect the IH formation for 0.1-0.1 and 0.9-0.9 columns, when the bigram repetition is at the Pareto frontier (0.1-0.3 column), only  $\text{Zipf}_{[+D+C]}$  results in the formation of IHs. The importance of skewed rank-frequency distributions, of which Zipfian distribution is an example, is also reported in Chan et al. (2022); Reddy (2024).

## 8. Discussion

### 8.1. Importance of task selection

Our results add a new piece of evidence to the growing body of literature on IHs, and on phase transition and emergence, more broadly. In Section 5, we find that larger context and batch sizes promote an earlier emergence of IHs. This seems to contradict with findings from Zucchet et al. (2025), where they find that the emergence of sparse attention, of which IH is a subtype, happens later with an increased context size. We suspect that this is due to a difference in the problem setup. Zucchet et al. (2025) uses the associative recall as a pretraining task, where a larger context size leads to more distance between the query and key tokens on average, and hence more distractor tokens in between. It is then sensible

<sup>4</sup>Under the  $-D$  conditions, IHs do seem to form with high repetition frequency and reliability (0.9-0.9) when measured in other metrics. See Section J.3 for the discussion.

that this leads to a later emergence of induction heads. Our setup, on the other hand, uses next token prediction as a pretraining task, where a larger context size naturally leads to more repetitions (see Figure 7), contributing to the earlier emergence of induction heads. On the topic of task selection, it is also worth noting that subword tokenization inflates the number of repeated bigrams in natural language, and using an orthographic tokenization might lead to different results, which is an interesting venue for future research.

### 8.2. Implication for broader phase transition

Phase transition is a broad term that refers to any abrupt change in a target behavior or metric of interest. It has been studied in the context of  $n$ -gram distributions (Chang et al., 2024; Chang & Bergen, 2025; Michaelov et al., 2025), human language processing (Aoyama & Wilcox, 2025), and concept space in vision (Okawa et al., 2023; Park et al., 2024), to name a few. Previous studies find that induction heads emerge after bigram learning (Olsson et al., 2022; Bietti et al., 2023). Although the present study focuses on IHs, and some aspects of the data distributional properties may be specific to them (e.g., repetitions), a broader trend observed in Section 5 may generalize to other behavioral phases in LM pretraining.

### 8.3. Conclusion

We showed that the emergence of IHs can be predicted by batch size and context size (Section 5). We also showed that the frequency and reliability of bigram repetitions can express a precise Pareto frontier below which IHs cease to form (Section 6). Lastly, we found that, among local dependency, categoriality, the shape of the marginal distribution, frequency, and reliability, none of them alone was a sufficient condition to ensure the formation of IHs (Section 7). However, we find that local dependency coupled with high frequency and reliability always result in IH formation, and that categoriality matters only when the frequency and reliability are close to the Pareto frontier. In this sense, natural language maintains a delicate balance of having sufficient bigram repetitions, while having both local dependency and categoriality, promoting the formation of IHs in LMs.

### 8.4. Limitation

As mentioned above, due to the limited compute resources, we only included models of up to 350M parameters in size for training, and 7B parameters for inference. Modern LMs are orders of magnitude larger in parameter count, and it is important to test if the trend holds for larger sizes. However, given a consistent trend we observed across three orders of magnitude (ranging from 50M GPT2 to 7B Pythia), we believe that a similar trend may hold for larger models.

## Impact Statement

This paper presents work whose goal is to advance the field of Machine Learning. There are many potential societal consequences of our work, none of which we feel must be specifically highlighted here.

## References

Aoyama, T. and Wilcox, E. Language models grow less humanlike beyond phase transition. In Che, W., Nabende, J., Shutova, E., and Pilehvar, M. T. (eds.), *Proceedings of the 63rd Annual Meeting of the Association for Computational Linguistics (Volume 1: Long Papers)*, pp. 24938–24958, Vienna, Austria, July 2025. Association for Computational Linguistics. ISBN 979-8-89176-251-0. URL <https://aclanthology.org/2025.acl-long.1214/>.

Biderman, S., Schoelkopf, H., Anthony, Q., Bradley, H., O'Brien, K., Hallahan, E., Khan, M. A., Purohit, S., Prashanth, U. S., Raff, E., Skowron, A., Sutawika, L., and van der Wal, O. Pythia: A suite for analyzing large language models across training and scaling. *arXiv preprint arXiv:2304.01373*, 2023. URL <https://arxiv.org/abs/2304.01373>.

Bietti, A., Cabannes, V., Bouchacourt, D., Jegou, H., and Bottou, L. Birth of a transformer: A memory viewpoint. In *Thirty-seventh Conference on Neural Information Processing Systems*, 2023. URL <https://openreview.net/forum?id=3X2EbBLNsk>.

Chan, S. C., Santoro, A., Lampinen, A. K., Wang, J. X., Singh, A. K., Richemond, P. H., McClelland, J., and Hill, F. Data distributional properties drive emergent in-context learning in transformers. In Oh, A. H., Agarwal, A., Belgrave, D., and Cho, K. (eds.), *Advances in Neural Information Processing Systems*, 2022. URL <https://openreview.net/forum?id=lHj-q9BSRjF>.

Chang, T. A. and Bergen, B. Bigram subnetworks: Mapping to next tokens in transformer language models. In *The Thirty-ninth Annual Conference on Neural Information Processing Systems*, 2025. URL <https://openreview.net/forum?id=0TD3e046gk>.

Chang, T. A., Tu, Z., and Bergen, B. K. Characterizing learning curves during language model pre-training: Learning, forgetting, and stability. *Transactions of the Association for Computational Linguistics*, 12:1346–1362, 2024. doi: 10.1162/tacl\_a\_00708. URL <https://aclanthology.org/2024.tacl-1.74/>.

Chen, A., Shwartz-Ziv, R., Cho, K., Leavitt, M. L., and Saphra, N. Sudden drops in the loss: Syntax acquisition, phase transitions, and simplicity bias in MLMs. In *The Twelfth International Conference on Learning Representations*, 2024. URL <https://openreview.net/forum?id=M05PiKHELW>.

Conneau, A., Khandelwal, K., Goyal, N., Chaudhary, V., Wenzek, G., Guzmán, F., Grave, E., Ott, M., Zettlemoyer, L., and Stoyanov, V. Unsupervised cross-lingual representation learning at scale. In Jurafsky, D., Chai, J., Schluter, N., and Tetreault, J. (eds.), *Proceedings of the 58th Annual Meeting of the Association for Computational Linguistics*, pp. 8440–8451, Online, July 2020. Association for Computational Linguistics. doi: 10.18653/v1/2020.acl-main.747. URL [https://aclanthology.org/2020.acl-main.747/](https://aclanthology.org/2020.acl-main.747).

Edelman, E., Tsilivis, N., Edelman, B. L., eran malach, and Goel, S. The evolution of statistical induction heads: In-context learning markov chains. In *The Thirty-eighth Annual Conference on Neural Information Processing Systems*, 2024. URL <https://openreview.net/forum?id=qaRT6QTIqJ>.

Ekbote, C., Makkula, A. V., Bondaschi, M., Rajaraman, N., Gastpar, M., Lee, J. D., and Liang, P. P. What one cannot, two can: Two-layer transformers provably represent induction heads on any-order markov chains. In *The Thirty-ninth Annual Conference on Neural Information Processing Systems*, 2025. URL <https://openreview.net/forum?id=nYg6Qzm5xS>.

Elhage, N., Nanda, N., Olsson, C., Henighan, T., Joseph, N., Mann, B., Askell, A., Bai, Y., Chen, A., Conerly, T., DasSarma, N., Drain, D., Ganguli, D., Hatfield-Dodds, Z., Hernandez, D., Jones, A., Kernion, J., Lovitt, L., Ndousse, K., Amodei, D., Brown, T., Clark, J., Kaplan, J., McCandlish, S., and Olah, C. A mathematical framework for transformer circuits. *Transformer Circuits Thread*, 2021. URL <https://transformer-circuits.pub/2021/framework/index.html>.

Groeneveld, D., Beltagy, I., Walsh, P., Bhagia, A., Kinney, R., Tafjord, O., Jha, A. H., Ivison, H., Magnusson, I., Wang, Y., Arora, S., Atkinson, D., Author, R., Chandu, K. R., Cohan, A., Dumas, J., Elazar, Y., Gu, Y., Hessel, J., Khot, T., Merrill, W., Morrison, J., Muenninghoff, N., Naik, A., Nam, C., Peters, M. E., Pyatkin, V., Ravichander, A., Schwenk, D., Shah, S., Smith, W., Strubell, E., Subramani, N., Wortsman, M., Dasigi, P., Lambert, N., Richardson, K., Zettlemoyer, L., Dodge, J., Lo, K., Soldaini, L., Smith, N. A., and Hajishirzi, H. Olmo: Accelerating the science of language models. *arXiv preprint arXiv:2402.00838*, 2024. URL <https://arxiv.org/abs/2402.00838>.

Kaplan, J., McCandlish, S., Henighan, T., Brown, T. B., Chess, B., Child, R., Gray, S., Radford, A., Wu, J., and

Amodei, D. Scaling laws for neural language models. *arXiv preprint arXiv:2001.08361*, 2020. URL <https://arxiv.org/abs/2001.08361>.

Michaelov, J. A., Levy, R. P., and Bergen, B. Language model behavioral phases are consistent across architecture, training data, and scale. In *The Thirty-ninth Annual Conference on Neural Information Processing Systems*, 2025. URL <https://openreview.net/forum?id=HepnVf03Wp>.

Nanda, N. and Bloom, J. Transformerlens. <https://github.com/TransformerLensOrg/TransformerLens>, 2022.

Oh, B.-D. and Schuler, W. Why does surprisal from larger transformer-based language models provide a poorer fit to human reading times? *Transactions of the Association for Computational Linguistics*, 11:336–350, 2023. doi: 10.1162/tacl\_a\_00548. URL <https://aclanthology.org/2023.tacl-1.20/>.

Okawa, M., Lubana, E. S., Dick, R. P., and Tanaka, H. Compositional abilities emerge multiplicatively: Exploring diffusion models on a synthetic task. In *Thirty-seventh Conference on Neural Information Processing Systems*, 2023. URL <https://openreview.net/forum?id=frVo9MzRuU>.

Olsson, C., Elhage, N., Nanda, N., Joseph, N., Das-Sarma, N., Henighan, T., Mann, B., Askell, A., Bai, Y., Chen, A., Conerly, T., Drain, D., Ganguli, D., Hatfield-Dodds, Z., Hernandez, D., Johnston, S., Jones, A., Kernion, J., Lovitt, L., Ndousse, K., Amodei, D., Brown, T., Clark, J., Kaplan, J., McCandlish, S., and Olah, C. In-context learning and induction heads. *Transformer Circuits Thread*, 2022. URL <https://transformer-circuits.pub/2022/in-context-learning-and-induction-heads/index.html>.

Park, C. F., Okawa, M., Lee, A., Lubana, E. S., and Tanaka, H. Emergence of hidden capabilities: Exploring learning dynamics in concept space. In *The Thirty-eighth Annual Conference on Neural Information Processing Systems*, 2024. URL <https://openreview.net/forum?id=owuEcT6BT1>.

Park, C. F., Lubana, E. S., and Tanaka, H. Competition dynamics shape algorithmic phases of in-context learning. In *The Thirteenth International Conference on Learning Representations*, 2025. URL <https://openreview.net/forum?id=XgH1wfHSX8>.

Radford, A., Wu, J., Child, R., Luan, D., Amodei, D., Sutskever, I., et al. Language models are unsupervised multitask learners. *OpenAI blog*, 1 (8):9, 2019. URL [https://cdn.openai.com/better-language-models/language\\_models\\_are\\_unsupervised\\_multitask\\_learners.pdf](https://cdn.openai.com/better-language-models/language_models_are_unsupervised_multitask_learners.pdf).

Reddy, G. The mechanistic basis of data dependence and abrupt learning in an in-context classification task. In *The Twelfth International Conference on Learning Representations*, 2024. URL <https://openreview.net/forum?id=aN4Jf6Cx69>.

Sanford, C., Hsu, D., and Telgarsky, M. One-layer transformers fail to solve the induction heads task. *arXiv preprint arXiv:2408.14332*, 2024. URL <https://arxiv.org/abs/2408.14332>.

Singh, A. K., Moskovitz, T., Hill, F., Chan, S. C., and Saxe, A. M. What needs to go right for an induction head? a mechanistic study of in-context learning circuits and their formation. In *Forty-first International Conference on Machine Learning*, 2024. URL <https://openreview.net/forum?id=08rrXl71D5>.

Wenzek, G., Lachaux, M.-A., Conneau, A., Chaudhary, V., Guzmán, F., Joulin, A., and Grave, E. CCNet: Extracting high quality monolingual datasets from web crawl data. In Calzolari, N., Béchet, F., Blache, P., Choukri, K., Cieri, C., Declerck, T., Goggi, S., Isahara, H., Maegaard, B., Mariani, J., Mazo, H., Moreno, A., Odijk, J., and Piperidis, S. (eds.), *Proceedings of the Twelfth Language Resources and Evaluation Conference*, pp. 4003–4012, Marseille, France, May 2020. European Language Resources Association. ISBN 979-10-95546-34-4. URL <https://aclanthology.org/2020.lrec-1.494/>.

Xie, S. M., Raghunathan, A., Liang, P., and Ma, T. An explanation of in-context learning as implicit bayesian inference. In *International Conference on Learning Representations*, 2022. URL <https://openreview.net/forum?id=RdJVFCjUMI>.

Yin, K. and Steinhardt, J. Which attention heads matter for in-context learning? *arXiv preprint arXiv:2502.14010*, 2025. URL <https://arxiv.org/abs/2502.14010>.

Zucchet, N., D’Angelo, F., Lampinen, A. K., and Chan, S. C. The emergence of sparse attention: impact of data distribution and benefits of repetition. In *The Thirty-ninth Annual Conference on Neural Information Processing Systems*, 2025. URL <https://openreview.net/forum?id=jMhRbV47pS>.

## A. Hyperparameters

Table 2. List of hyperparameters used to train LMs.

Architecture			
name	GPT2 50M	GPT2 125M	GPT2 350M
vocab_size	50,257	50,257	50,257
context_size	4–2048	32–2048	32–2048
d_embed	768	1,024	1,024
d_ffn	3,072	4,096	4,096
n_layer	2	12	24
n_head	8	12	16
activation	gelu	gelu	gelu
num_params	50M	125M	350M
Training			
train_size	1B	1B	1B
num_epoch	1	1	1
train_amount	1B	1B	1B
batch_size	4–512	16–256	16–256
weight_decay	0.1	0.1	0.1
warmup_steps	1%	1%	1%
lr	5e-4	5e-4	5e-4
lr_scheduler	cosine	cosine	cosine

We also include 6 Pythia models: 70M, 160M, 410M, 1B, 2.8B, and 6.9B. For the details of these Pythia models, see Table 1 of [Biderman et al. \(2023\)](#).

## B. Determining the threshold for random attention

In Figure 2 (center), the lines representing context sizes of 4, 8, and 16 seem to be somewhat flat, meaning that the model does not improve in its ability to attend back to the token necessary to complete the repeated bigram. The high PSs associated with these models are simply due to the higher attention preceding tokens can get by chance; with the context size of 4, for example, the model has at most 4 tokens to attend back to, with the random attention of 0.25.

To systematically determine what counts as “above random,” we simulate the random attention over previous tokens via Markov Chain Monte-Carlo (MCMC) using a Dirichlet distribution with a uniform prior. We find that attention weights as strong as 0.72, 0.35, and 0.16 are necessary for models with context sizes of 4, 8, and 16, respectively, to be considered *above random* at the alpha level of 0.01. Hence, we conclude that these three context sizes do not promote the formation of IHs, and in the remaining analyses in this subsection, we will focus on the rest of the models.

## C. Figure 2 plotted against the number of training tokens

In Figure 2, we plotted how batch size, context size, and bigram repetition rate affect the formation point of IHs, measured in the number of training steps. Trivially, models with different batch sizes and context sizes will have been exposed to different numbers of tokens at the same training step. This could raise the question of whether or not the observed shifting effect is just an artifact of the total number of training tokens being different on the same point on the *x*-axis. Hence, we show the same graph plotted against the number of total training tokens, instead of the number of training steps in Figure 6. Here again, we observe the shifting effect, but in the opposite direction: the smaller the batch/context size, the earlier the phase transition point. Therefore, we can say that, even when measured in the number of training tokens, IHs form at different points when we change batch size and/or context size, ruling out the possibility that the observed shifting effect in Figure 2 is an artifact of each point on *x*-axis representing a different number of pretraining *tokens*.

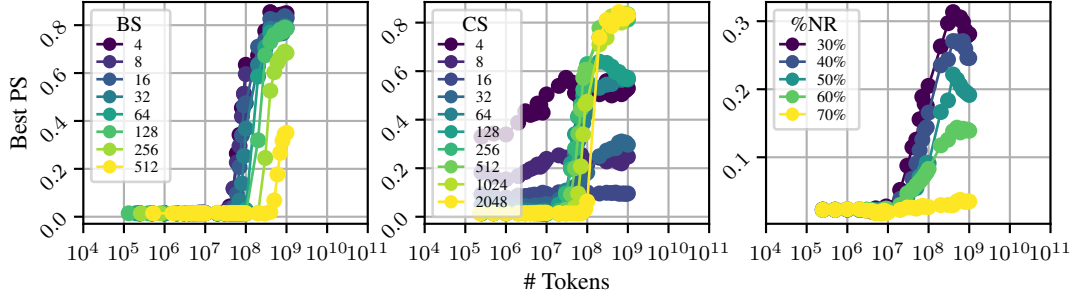


Figure 6. Developmental trajectories of PS of LMs with various batch sizes (left), context sizes (center), and repetitions (right) over the course of 1B tokens of pretraining, plotted against the number of updates (a) and the number of tokens (b). BS, CS, %NR stands for batch size, context size, and the proportion of chunks with no repetitions, respectively.

## D. Fitting procedure for the prediction of emergence points

Here, we provide details on the procedure for fitting a regression model to predict emergence points.

### D.1. Emergence points

First, given a metric of interest that goes through an abrupt change, we need a way to systematically identify the point (in number of training steps or tokens) at which it is said to go through a phase transition point (or a certain capability measured by the score “emerges”). A few different approaches, such as the sharpest slope (Chen et al., 2024), and the first point at which the metric exceeds a given threshold (Aoyama & Wilcox, 2025). Here, given a curve that shows the development of a given metric’s score over the course of some time metric, such as training steps and tokens (e.g., Figure 6), we fit a piece-wise liner function (PWLF) model to the curve with three segments. We choose three as we observe the initial stagnation phase, where the score is around 0, the abrupt improvement phase, and the eventual plateau phase. We then take the “knot” between the first two segments and operationalize that point as the emergence point.

### D.2. Data for fitting the linear regression models

The aforementioned emergence identification assigns a single emergence point for each model. Hence, we have as many data points as models. We have trained GPT2-50M models with 18 different batch and context size configurations (Section 5), as well as GPT2-125M and GPT-350M with 7 different configurations each. However, because we have shown that emergence was not observed in the context sizes of {4, 8, 16}, we exclude those models in this analysis. We finally add 6 Pythia models {70M, 160M, 410M, 1B, 2.8B, 6.9B} all trained on batch size of 1024 and context size of 2048. In total, we fit a regression model on these 35 models. We reported the “fit” of this regression model trained on all of the data points; however, we also report the results from cross-fold validation as well in Table 5.

### D.3. Regression model details for phase transition prediction

In Section 5, we fitted a linear regression in log space using batch size, context size, and model size as predictors for the phase transition point.

Table 3 summarizes the linear regression model with all three predictors. A few consistent trends emerge: first, batch size and context size are (1) statistically significant across the board, regardless of the metric used to define the phase transition point, and (2) in the negative direction, meaning that the increase in these predictors *slow down* the emergence. Second, model size is non-significant across the board, regardless of the metric. Hence, we conclude that the emergence points are independent of model size. The final regression models without the model size are summarized in Table 4.

Lastly, as mentioned earlier, we also report the results of 5-fold cross-validation of the full regression models and the models without model size in Table 5. Each fold trains the regression model on 80% of the training data (28 models) and predicts the emergence points of the remaining 20% of the data (7 models). Most test  $R^2$ ’s range from 0.8 to 0.9, indicating an excellent

Table 3. A summary of linear regression analyses with an intercept, logB (batch size), logC (context size), and logS (model size) as independent variables and the phase transition point (in the number of updates) in each of the four metrics, PS, LA, AR (accuracy), AR (mean rank), as dependent variables.

<b>y</b>	<b>x</b>	<b>coef</b>	<b>std err</b>	<b>t</b>	<b>p</b>	<b>95% CI</b>
<b>PS</b>	<b>Intercept</b>	13.2700	0.468	28.326	0.000	12.315 14.225
	<b>logB</b>	-0.3683	0.044	-8.318	0.000	-0.459 -0.278
	<b>logC</b>	-0.6149	0.073	-8.411	0.000	-0.764 -0.466
	<b>logS</b>	-0.0027	0.063	-0.043	0.966	-0.130 0.125
<b>LA</b>	<b>Intercept</b>	13.6083	0.477	28.529	0.000	12.635 14.581
	<b>logB</b>	-0.3735	0.045	-8.286	0.000	-0.465 -0.282
	<b>logC</b>	-0.6461	0.074	-8.678	0.000	-0.798 -0.494
	<b>logS</b>	-0.0069	0.064	-0.108	0.915	-0.137 0.123
<b>AR (accuracy)</b>	<b>Intercept</b>	16.3236	0.632	25.846	0.000	15.036 17.612
	<b>logB</b>	-0.5885	0.060	-9.859	0.000	-0.710 -0.467
	<b>logC</b>	-0.7925	0.099	-8.040	0.000	-0.993 -0.591
	<b>logS</b>	-0.0154	0.084	-0.182	0.856	-0.188 0.157
<b>AR (mean rank)</b>	<b>Intercept</b>	12.3780	0.723	17.125	0.000	10.904 13.852
	<b>logB</b>	-0.5194	0.068	-7.603	0.000	-0.659 -0.380
	<b>logC</b>	-0.4928	0.113	-4.369	0.000	-0.723 -0.263
	<b>logS</b>	0.1295	0.097	1.340	0.190	-0.068 0.327

fit to the *held-out* data points. Note that  $R^2_{test}$  is computed as:

$$1 - \frac{SS_{residual}}{SS_{total}} \quad (12)$$

and the value of 1 indicates a perfect prediction on the test set.

Table 4. A summary of linear regression analyses with an intercept, logB (batch size), and logC (context size) as independent variables and the phase transition point (in the number of updates) in each of the four metrics, PS, LA, AR (accuracy), AR (mean rank), as dependent variables.

y	x	coef	std err	t	p	95% CI	
PS	<b>Intercept</b>	13.2630	0.432	30.666	0.000	12.382	14.144
	<b>logB</b>	-0.3689	0.041	-9.010	0.000	-0.452	-0.286
	<b>logC</b>	-0.6155	0.071	-8.694	0.000	-0.760	-0.471
LA	<b>Intercept</b>	13.5904	0.440	30.856	0.000	12.693	14.488
	<b>logB</b>	-0.3752	0.042	-8.999	0.000	-0.460	-0.290
	<b>logC</b>	-0.6475	0.072	-8.981	0.000	-0.794	-0.501
AR (accuracy)	<b>Intercept</b>	16.2837	0.583	27.913	0.000	15.095	17.472
	<b>logB</b>	-0.5922	0.055	-10.723	0.000	-0.705	-0.480
	<b>logC</b>	-0.7957	0.095	-8.333	0.000	-0.990	-0.601
AR (mean rank)	<b>Intercept</b>	12.7138	0.686	18.525	0.000	11.316	14.112
	<b>logB</b>	-0.4880	0.065	-7.511	0.000	-0.620	-0.356
	<b>logC</b>	-0.4656	0.112	-4.145	0.000	-0.694	-0.237

Table 5. Cross-fold validation results for the full regression model (left) and the regression model without model size (right). Each fold trains the regression model on 80% of the data and predicts on the remaining 20% of the data. Recall that  $\beta$ ,  $\gamma$ ,  $\theta$  are coefficients of batch size, context size, and model size, respectively. Prediction quality is measured in  $R^2_{test} = \frac{SS_{residual}}{SS_{total}}$

Metric	Fold	Full				w/o Model Size		
		$\beta$	$\gamma$	$\theta$	$R^2_{test}$	$\beta$	$\gamma$	$R^2_{test}$
PS	1	-0.3663	-0.6223	0.0130	0.7629	-0.3617	-0.6204	0.7653
	2	-0.3517	-0.5380	-0.0055	0.8969	-0.3527	-0.5387	0.8966
	3	-0.3607	-0.6232	0.0033	0.9282	-0.3600	-0.6222	0.9284
	4	-0.4000	-0.6023	0.0026	0.8338	-0.3992	-0.6019	0.8340
	5	-0.3775	-0.6438	-0.0167	0.8204	-0.3811	-0.6478	0.8234
LA	1	-0.3713	-0.6599	0.0101	0.7629	-0.3677	-0.6584	0.7649
	2	-0.3627	-0.5386	-0.0127	0.8871	-0.3649	-0.5403	0.8864
	3	-0.3724	-0.6585	-0.0004	0.9056	-0.3725	-0.6586	0.9055
	4	-0.3933	-0.6364	-0.0032	0.8818	-0.3943	-0.6369	0.8816
	5	-0.3829	-0.6811	-0.0171	0.8073	-0.3866	-0.6852	0.8092
AR (accuracy)	1	-0.5963	-0.7979	0.0176	0.7907	-0.5900	-0.7952	0.7942
	2	-0.5866	-0.6605	-0.0283	0.9060	-0.5916	-0.6643	0.9055
	3	-0.5762	-0.8585	0.0488	0.8115	-0.5670	-0.8437	0.8257
	4	-0.6115	-0.7897	-0.0189	0.9417	-0.6171	-0.7924	0.9418
	5	-0.5897	-0.7847	-0.1022	0.8923	-0.6117	-0.8093	0.9353
AR (mean rank)	1	-0.5660	-0.4922	0.1891	0.7325	-0.4989	-0.4634	0.8427
	2	-0.4967	-0.5753	0.1073	0.7413	-0.4778	-0.5608	0.7146
	3	-0.5175	-0.4716	0.1340	0.8988	-0.4922	-0.4309	0.8876
	4	-0.5770	-0.4459	0.1659	0.8104	-0.5273	-0.4216	0.8597
	5	-0.4477	-0.4918	0.0377	0.6032	-0.4396	-0.4827	0.5866

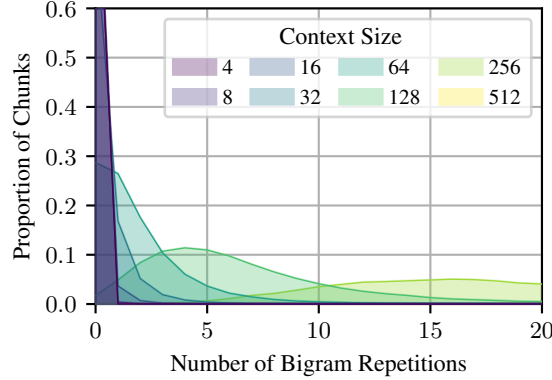


Figure 7. Smoothed distribution of chunks with various numbers of bigram repetitions. Context sizes 1024 and 2048 were rendered invisible, and hence removed from the plot. The plot is truncated at  $y=0.6$  for readability, but context sizes of 4, 8, and 16 had  $>95\%$  of chunks with no bigram repetitions.

## E. Distribution of bigram repetitions with various context sizes

Since adding or removing bigrams in naturally occurring texts introduces noise, such as broken syntax, we manipulate the frequency of repeated bigrams in natural language data by first putting tokenized texts into chunks of  $c$ , where  $c$  is the context size of the LM, and then selecting those natural chunks to ensure  $p\%$  of the chunks of the resulting training data include no bigram repetition at all, where  $p$  is the parameter we can control. Modern LMs have a context size of at least 1024. However, in naturally occurring texts, sequences of 1024 tokens without any repeated bigrams  $\langle A, B, \dots, A, B \rangle$  in them are very rare, if not non-existent. In general, as shown in Figure 7, larger context size trivially tends to contain more repeated bigrams, and we find that the context size of 64 strikes the balance between including enough context and containing a good number of chunks with and without repeated bigrams. Hence, in Section 6 and Section 7, we use LMs with a context size of 64.

## F. Frequency $P(A, B, \dots, A)$ and Reliability $P(B | A, B, \dots, A)$

Recall that Elhage et al. (2021); Olsson et al. (2022) define IHs as specific heads that complete the repeated  $\langle A, B, \dots, A, B \rangle$  sequence when seeing  $\langle A, B, \dots, A \rangle$ . As a naive hypothesis, we speculate that the presence of repeated bigrams (separated by an arbitrarily long sequence of tokens within the LM’s context size) is essential for IH formation. Consider the following sequence, which we will use as a running example: In this example, there are 4 tokens that occur more than once (i.e., **A**, **B**, **E**, **F**). For the first occurrence of these 4 tokens, each of them is followed by *something*; for example, **A** is followed by **B**, and **B** is followed by **C**. For the second occurrence of these 4 tokens, one can induce that a bigram tends to repeat *in-context*, if these 4 tokens are reliably followed by what followed them the first time they occurred; namely, if **A**, **B**, **E**, **F**, are followed by **B**, **C**, **F**, **A**, respectively. In Table 6, there exist 4 such opportunities for learning the bigram repetition, and 2 such opportunities actually reward such learning, since only the second occurrences of **A** and **E** are followed by the same bigram continuations of their first occurrences. Here, we have touched upon the two knobs we aim to define here. **Frequency** involves the tokens that are of the word type occurring for the  $n$ -th time where  $n \geq 2$  (**A**, **B**, **E**, **F** in Table 6). **Reliability** measures, of all such tokens, how many of them actually complete the same bigram continuation (**B**, **E** in Table 6). We will now define each of these two measures formally.

Table 6.  $R_U$  and  $R_B$  of an example sequence. This sequence has a  $P(R_U) = \frac{4}{10}$  and  $P(R_B) = \frac{2}{10}$ , hence **frequency** and **reliability** are 0.4 and 0.5, respectively.

Word	A	B	C	D	E	F	A	B	E	F
$R_U$	0	0	0	0	0	0	1	1	1	1
$R_B$	0	0	0	0	0	0	1	0	1	0

**Frequency**: given a binary variable *unigram repetition*  $R_U \in \{0, 1\}$ , whose value is 1 if a given token is the second

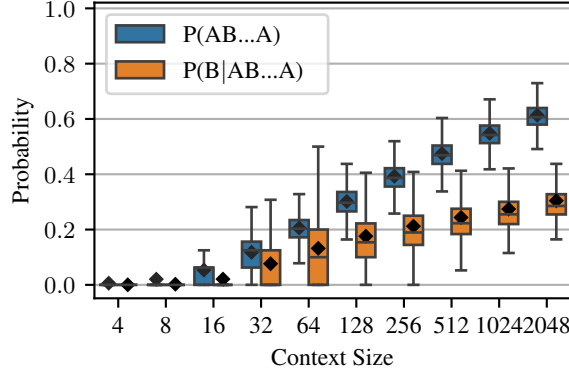


Figure 8. Distribution of chunks with various  $P(A, B, \dots, A)$  and  $P(B | A, B, \dots, A)$  for each context size. Only the quartile box, median (center line in each box), mean (diamond), and whiskers are shown, and Outliers are not shown for readability.

occurrence of A of the  $\langle A, B, \dots, A \rangle$  sequence (i.e., a repeated unigram), and 0 otherwise, we define ‘‘frequency’’ as  $P(R_U)$ . Informally, in the induction term, this is  $P(A, B, \dots, A)$ , or the rate at which  $\langle A, B, \dots, A \rangle$  sequence is encountered. In practice, this is equivalent to the sum of all unigram counts in a given sequence, with the first occurrence removed:

$$P(A, B, \dots, A) = \frac{1}{|\mathcal{S}|} \sum_{w \in \mathcal{V}} \max(c(w, \mathcal{S}) - 1, 0) \quad (13)$$

where  $\mathcal{V}$  is the vocabulary, or the set of all possible unigrams, and  $c(w, \mathcal{S})$  is a count of a word  $w$  in a sequence  $\mathcal{S}$  of the same size as the model’s context size. In Table 6, we saw 4 such tokens (tokens where  $R_U = 1$ :  $A, B, E, F$ ) in the context of size 10, hence  $P(R_U) = P(A, B, \dots, A) = \frac{4}{10}$ . Technically, consecutive occurrences of a given token type should not be counted; however, this does not happen frequently in the real data, and no tokens were allowed to occur twice in a row in synthetic data, trivializing this problem (see Algorithm 1).

**Reliability:** given a binary variable *bigram repetition*  $R_B \in \{0, 1\}$ , whose value is 1 if a given token’s *next token* is the second occurrence of B of the  $\langle A, B, \dots, A, B \rangle$  sequence (i.e., a repeated bigram), and 0 otherwise, I define ‘‘reliability’’ as  $\frac{P(R_B)}{P(R_U)}$ . Informally, in induction term,  $P(R_B)$  is  $P(A, B, \dots, A, B)$ , and reliability, or  $\frac{P(R_B)}{P(R_U)}$ , is equivalent via the chain rule to the conditional probability  $P(B | A, B, \dots, A)$ : the rate at which an  $\langle A, B, \dots, A \rangle$  sequence is followed by B:

$$P(B | A, B, \dots, A) = \frac{P(A, B, \dots, A, B)}{P(A, B, \dots, A)} = \frac{P(R_B)}{P(R_U)} = \frac{\frac{1}{|\mathcal{S}|} \sum_{b \in \mathcal{B}} \max(c(b, \mathcal{S}) - 1, 0)}{\frac{1}{|\mathcal{S}|} \sum_{w \in \mathcal{V}} \max(c(w, \mathcal{S}) - 1, 0)} \quad (14)$$

where  $\mathcal{B}$  denotes the set of all possible bigrams, and  $c(b, \mathcal{S})$  the count of the bigram  $b$  in a given sequence  $\mathcal{S}$ . In Table 6, of all the 10 positions (tokens), 2 completed the  $\langle A, B, \dots, A, B \rangle$  sequence (tokens where  $R_B = 1$ : second occurrences of B and F), hence  $P(R_B) = P(A, B, \dots, A, B) = \frac{2}{10}$ . Therefore, reliability is  $\frac{2}{10} \div \frac{4}{10} = \frac{1}{2}$ . It might make more intuitive sense to compute this directly without using the chain rule: of all the 4 tokens that complete the  $\langle A, B, \dots, A \rangle$  sequence, 2 of them are followed by B, hence  $\frac{2}{4} = \frac{1}{2}$ . Equivalently, of the tokens where  $R_U = 1$  in Table 6, half of them also have  $R_B = 1$ . However, for the computational purpose, the chain rule is much simpler, which is the reason we introduced the chain rule based calculation above. In this study, ‘‘frequency’’ and  $P(A, B, \dots, A)$  are used interchangeably, and so are ‘‘reliability’’ and  $P(B | A, B, \dots, A)$ .

Note that this is a more precise characterization of what Chan et al. (2022) called ‘‘burstiness.’’ In their formulation, where the task was to predict the label of an image given image-label pairs in-context, a ‘‘bursty’’ sequence contains certain image-label pairs more often than others, while controlling for the marginal distribution over all sequences. This is effectively equivalent to increasing both frequency and reliability in our terms. Two sequences of image-label pairs ( $I_i, L_i$ ):  $\langle I_1, L_1, I_2, L_2, I_3, L_3, I_4, L_4 \rangle$  (non-bursty) and  $\langle I_1, L_1, I_2, L_2, I_1, L_1, I_3, L_3 \rangle$  (bursty) can be reformulated as  $\langle A, B, C, D, E, F, G, H \rangle$  and  $\langle A, B, C, D, A, B, E, F \rangle$ , respectively, and the former has frequency and reliability of 0, whereas the latter has frequency and reliability of 1/8 and 1/2 ( $\langle A, B, \dots, A \rangle$  is followed by B, but  $\langle B, C, \dots, B \rangle$  is not followed by C), respectively. We can verify that natural texts with various chunk sizes are not only different in terms of the number of repeated bigrams (as shown in Figure 7), but also in the two probabilities defined above. Figure 8 confirms

this: both  $P(A, B, \dots, A)$  and  $P(B | A, B, \dots, A)$  increases as the context size increases. While  $P(A, B, \dots, A)$  seems to increase log-linearly ( $x$ -axis is in log scale), the increase in  $P(B | A, B, \dots, A)$  seems to slow down. Since IHs were not forming, or very weak at most, for context size of 32, we speculate that the threshold values of  $P(A, B, \dots, A)$  and  $P(B | A, B, \dots, A)$  to be somewhere between 0.1–0.2, and 0.1–0.15, respectively.

## G. Algorithm for Frequency- and Reliability-Constrained Training Data Generation

**Algorithm 1** Corpus generation constrained on  $P(A, B, \dots, A)$  and  $P(B | A, B, \dots, A)$

Sample a token sequence  $\mathbf{s}$  from the distribution  $\mathcal{D} : \{w \mapsto \mathcal{D}_w \in \mathbb{R}^{|\mathcal{V}|} \mid w \in \mathcal{V}\}$ ,  
 constrained on  $\alpha = P(A, B, \dots, A)$  and  $\beta = P(B | A, B, \dots, A)$

---

```

1: Input: ctx_size,  $\mathcal{V}, \mathcal{D} \in \mathbb{R}^{|\mathcal{V}| \times |\mathcal{V}|}$ ,  $\alpha, \beta$ 
2:  $\mathbf{s} \leftarrow []$  ▷ init a token sequence
3:  $\mathcal{U}_t \leftarrow \{\}$  ▷ init a unigram set at step  $t$ 
4:  $\mathcal{B}_t \leftarrow \{\}$  ▷ init a bigram continuation dict  $\{w \mapsto \mathcal{B}_t(w) \mid w \in \mathcal{U}_t\}$  at step  $t$ 
5:  $m \leftarrow \text{ctx\_size} // 2$  ▷ first half
6: for  $t$  from 1 to  $m$  do
7:    $w_t \sim \mathcal{D}_{w_{t-1}}(\mathcal{V} \setminus \mathcal{U}_{t-1})$ 
8:   add  $w_t$  to  $\mathbf{s}$ 
9:   update  $\mathcal{U}_t$  and  $\mathcal{B}_t$ 
10:  for  $t$  from  $m$  to  $\text{ctx\_size}$  do ▷ second half
11:    is_aba  $\leftarrow w_t$  in  $\mathcal{U}_{t-1}$ 
12:    make_aba  $\leftarrow \text{random.random}() \leq \alpha$  ▷  $\alpha$  represents  $P(A, B, \dots, A)$ 
13:    make_abab  $\leftarrow \text{random.random}() \leq \beta$  ▷  $\beta$  represents  $P(B | A, B, \dots, A)$ 
14:    if is_aba( $w_t$ ) then
15:      if make_abab then
16:         $w_t \sim \mathcal{D}_{w_{t-1}}(\cdot \mid \mathcal{B}_t(w_{t-1}))$ 
17:      else
18:        if make_aba then
19:           $w_t \sim \mathcal{D}_{w_{t-1}}(\cdot \mid \mathcal{U}_{t-1} \setminus \mathcal{B}_t(w_{t-1}))$ 
20:        else
21:           $w_t \sim \mathcal{D}(\cdot \mid \mathcal{V} \setminus \{\mathcal{U} \cup \mathcal{B}_t(w_{t-1})\})$ 
22:      else
23:        if make_aba then
24:           $w_t \sim \mathcal{D}_{w_{t-1}}(\cdot \mid \mathcal{U}_{t-1})$ 
25:        else
26:           $w_t \sim \mathcal{D}_{w_{t-1}}(\cdot \mid \mathcal{V} \setminus \mathcal{U}_{t-1})$ 
27:    add  $w_t$  to  $\mathbf{s}$ 
28:    update  $\mathcal{U}_t$  and  $\mathcal{B}_t$ 

```

---

To fully control the two properties, frequency  $P(A, B, \dots, A)$  and reliability  $P(B | A, B, \dots, A)$  in text data, we need a way to sample words from some distribution, while enforcing desired values of these two knobs. To this end, we approximate natural language by first tokenizing texts from the English subcorpus of the Common Crawl Corpus (CC100; Conneau et al., 2020; Wenzek et al., 2020) and collecting token bigram statistics. We then create a token-to-token transition matrix  $T \in \mathbb{R}^{|\mathcal{V}| \times |\mathcal{V}|}$ , where  $\mathcal{V}$  is the vocabulary. We use off-the-shelf GPT2 tokenizer, but reduced the vocabulary size to 10,000.

In Algorithm 1, we outline the semi-synthetic data generation algorithm, where  $(\mathcal{A} \setminus \mathcal{B})$  denotes an asymmetric difference, or a set of elements in  $\mathcal{A}$  but not in  $\mathcal{B}$ ,  $\{x \mid x \in \mathcal{A} \text{ and } x \notin \mathcal{B}\}$ .  $\mathcal{U}_{t-1}$  is a set of unigrams attested before time step  $t-1$ , and  $\mathcal{B}_x$  denotes a set of attested bigram continuations of token  $x$ . The idea is that we first generate the first half of the sequence by randomly walking through the Markov chain. This is to ensure that a sufficient number of unique tokens are present in the sequence before the restricted generation can take place; otherwise, Algorithm 1 often produces degenerate sequences especially with high values of  $P(A, B, \dots, A)$  and  $P(B | A, B, \dots, A)$ . For the second half, based on the condition (if the prefix constitutes  $\langle A, B, \dots, A \rangle$ ) and constraints (to make a new  $\langle A, B, \dots, A \rangle$  and/or  $\langle A, B, \dots, A, B \rangle$ ), the word at each time step  $w_t$  is sampled from the distribution  $\mathcal{D}$  restricted to some subset  $\mathcal{S}$  that satisfies the conditions and constraints. For

simplicity, no tokens were allowed to occur consecutively.

## H. Matrix Optimization

In Section 7, we defined the underlying Markov Processes as transition matrices, which were then used to generate synthetic data, via a set of desired properties. These transition matrices were optimized using the Adam optimizer to satisfy the desired properties as closely as possible.

$$\mathcal{L} = \lambda_1 \mathcal{L}_D + \lambda_2 \mathcal{L}_E + \lambda_3 \mathcal{L}_P + \lambda_4 \mathcal{L}_{WC} + \lambda_5 \mathcal{L}_{WA} \quad (15)$$

where the 5 terms correspond to distribution loss, entropy loss, peakedness loss, within-category loss, and across-category loss, respectively. The 5  $\lambda$ s correspond to the weighting factors.

**Distribution loss ( $\mathcal{L}_D$ ).** This term is to ensure the transition matrix  $T \in \mathbb{R}^{|\mathcal{V}| \times |\mathcal{V}|}$  has a marginal distribution of the desired shape (Uniform, Gaussian, or Zipfian, as discussed in Section 7). We penalize the divergence from the desired shape by including KL divergence between the actual marginal distribution and the desired distribution:

$$\mathcal{L}_D = \sum_{i=1}^{|\mathcal{V}|} P(w_i) \frac{\log P(w_i)}{\log Q(w_i)}, \quad (16)$$

where  $P$  and  $Q$  are desired and actual marginal distributions, respectively.

**Entropy loss ( $\mathcal{L}_E$ ).** This term is to ensure each transition matrix is comparable in predictability. Because a transition matrix sampled from natural language had the entropy of  $\approx 6.2$ , we set the target entropy value to be 6.2, and included the squared difference as a loss term:

$$\mathcal{L}_E = \|H_{\text{target}} - H(T)\|_2^2, \quad (17)$$

where the estimation of  $H(T)$  is detailed in Appendix I.

**Peakedness loss ( $\mathcal{L}_P$ ).** We find that the matrix optimization often suffers from a degenerate matrix, where the desired properties are satisfied by allocating a very large probability mass to a single token in each row. To mitigate this problem, we include the mean of row-wise largest probabilities:

$$\mathcal{L}_P = \frac{1}{|\mathcal{V}|} \sum_{i=1}^{|\mathcal{V}|} \max T_{i,:}, \quad (18)$$

where  $T_{i,:}$  is the  $i$ -th row of the matrix  $T$ .

**Within-category loss ( $\mathcal{L}_{WC}$ ) and across-category loss ( $\mathcal{L}_{AC}$ ).** As defined in Section 7, the within-category similarity is the mean similarity of all pairs of words within a category, whereas the across-category similarity is the mean similarity of all pairs of words from different categories. For the +C configuration, we set the target within- and across-category similarities to be 0.4 and 0.1, respectively, and both were set to be 0.1 for the -C configuration. The squared differences between the actual and desired within/across category similarities were included as loss terms. The within-category loss is defined as:

$$\mathcal{L}_{WC} = \|\text{WC}_{\text{target}} - \text{WC}(T)\|_2^2, \quad (19)$$

where WC is within-category similarity:

$$\frac{1}{N} \sum_{c \in C} \sum_{w, w' \in c, w \neq w'} \text{sim}(w, w') \quad (20)$$

Similarly, across-category loss is defined as:

$$\mathcal{L}_{AC} = \|\text{AC}_{\text{target}} - \text{AC}(T)\|_2^2, \quad (21)$$

where AC is across-category similarity:

$$\frac{1}{N} \sum_{c, c' \in C, c \neq c'} \sum_{w \in c} \sum_{w' \in c'} \text{sim}(w, w') \quad (22)$$

We optimize the matrix with these loss terms for 5,000 steps with  $\lambda_1 = 100$ ,  $\lambda_2 = 0.01$ ,  $\lambda_3 = 0.1$ ,  $\lambda_4 = \lambda_5 = 5$ .

## I. Conditional Entropy

Conditional entropy is defined as:

$$H(X | Y) = \sum_{y \in Y} P(y) \left[ \sum_{x \in X} P(x | y) \log \frac{1}{P(x | y)} \right] \quad (23)$$

For a transition matrix  $T \in \mathbb{R}^{|\mathcal{V}| \times |\mathcal{V}|}$ , where  $\mathcal{V}$  is the vocabulary, it can be expressed as:

$$H(T) = \sum_{i=1}^{|\mathcal{V}|} P(w_i) \left[ \sum_{j=1}^{|\mathcal{V}|} P(w_j | w_i) \log \frac{1}{P(w_j | w_i)} \right] \quad (24)$$

Since the transition matrix  $T$  is a row-stochastic matrix, and each row sums to 1, the conditional probability  $P(w_j | w_i)$  is an entry  $T[i, j]$ . The marginal probability  $P(w_i)$  can be estimated by obtaining the stationary distribution of the transition distribution  $T$ , which is a left eigenvector with the eigenvalue of 1. Assume a ground-truth stationary distribution  $\pi$ ; this stationary distribution, which is the unigram distribution the transition matrix converges to, should remain unchanged after transitions:

$$\pi T = \pi \quad (25)$$

Eigenvector is a vector that only gets scaled by a factor  $\lambda$  after a linear transformation  $L$ . Hence, we can find the stationary unigram distribution  $\pi$  by finding the left eigenvector with the eigenvalue of 1 of a linear transformation  $T$ .

Now that we have the stationary distribution  $\pi$ , Equation (24) can be expressed as a matrix multiplication:

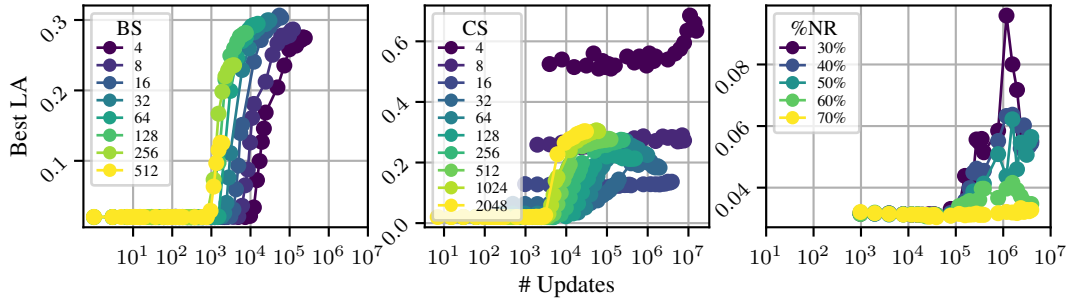
$$H(T) = \sum_{i=1}^{|\mathcal{V}|} \pi[i] \cdot H(T[i, :]) \quad (26)$$

## J. Analyses with other metrics

### J.1. Experiment 1

We replicate the analyses from Section 5 in other metrics: LA in Figure 9a and Figure 9b), AR (accuracy) in Figure 10a and Figure 10b, and AR (mean rank) in Figure 11a and Figure 11b. Notably, the shifting and slanting effects discussed in Section 5 are visibly captured by LA (Figure 9a) and by AR (mean rank; Figure 11a), but not as pronounced in AR (accuracy; Figure 10a). This is presumably, again, due to the discrete nature of accuracy, where the metric only captures whether the model ranks the target token as the most probable token or not. Another point worth noting is that, AR (accuracy) gives a false impression that a batch size of 512 fails in the associative recall task, as shown by the yellow curve in Figure 9a. However, when looking at the mean rank as opposed to accuracy, we can see that it goes through an abrupt drop (improvement) in the model trained with a batch size of 512 (Figure 11a), highlighting the importance of analyzing multiple metrics.

(a)



(b)

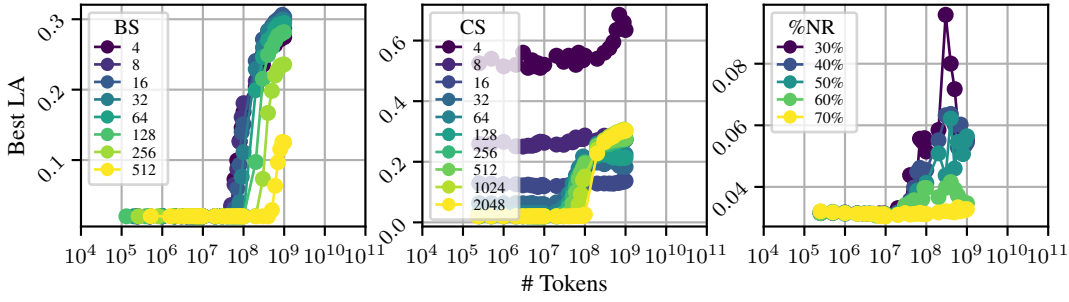
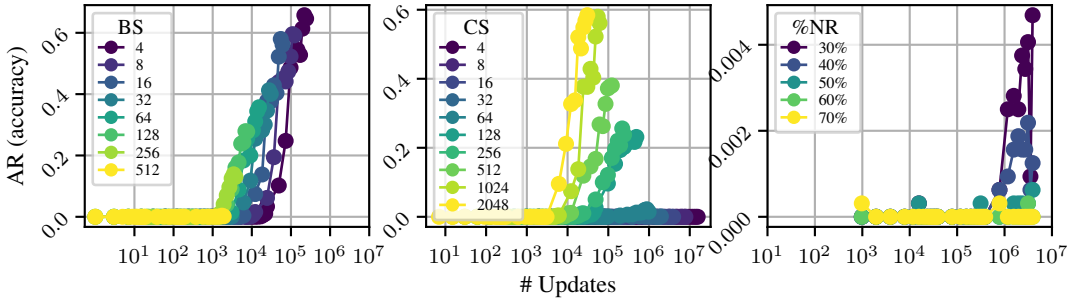


Figure 9. Developmental trajectories of LA of LMs with various batch sizes (left), context sizes (center), and repetitions (right) over the course of 1B tokens of pretraining, plotted against the number of updates (a) and the number of tokens (b). BS, CS, %NR stands for batch size, context size, and the proportion of chunks with no repetitions, respectively.

(a)



(b)

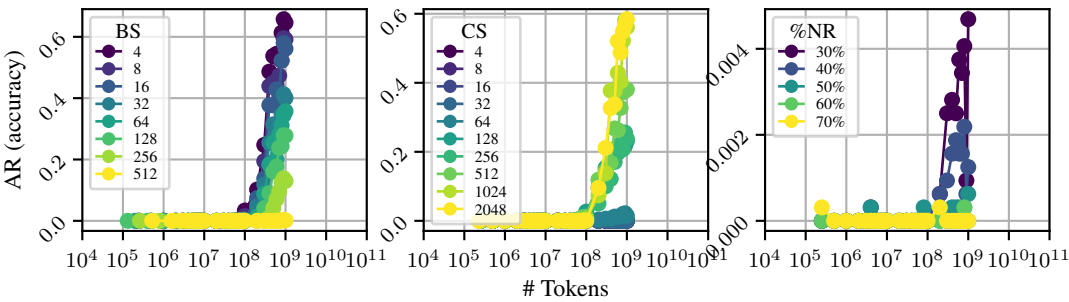
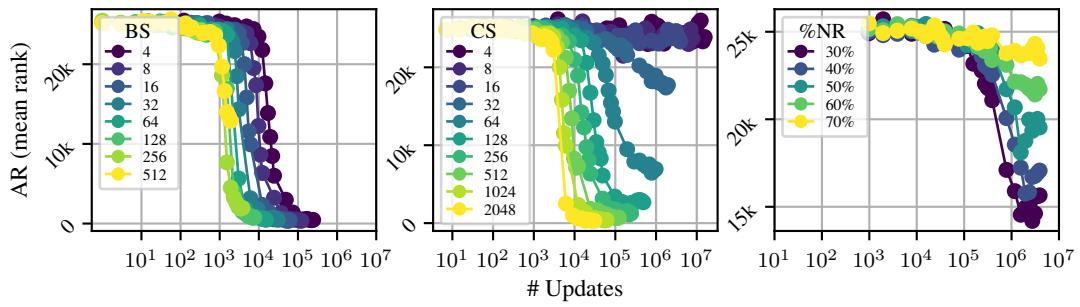


Figure 10. Developmental trajectories of AR (accuracy) of LMs with various batch sizes (left), context sizes (center), and repetitions (right) over the course of 1B tokens of pretraining, plotted against the number of updates (a) and the number of tokens (b). BS, CS, %NR stands for batch size, context size, and the proportion of chunks with no repetitions, respectively.

(a)



(b)

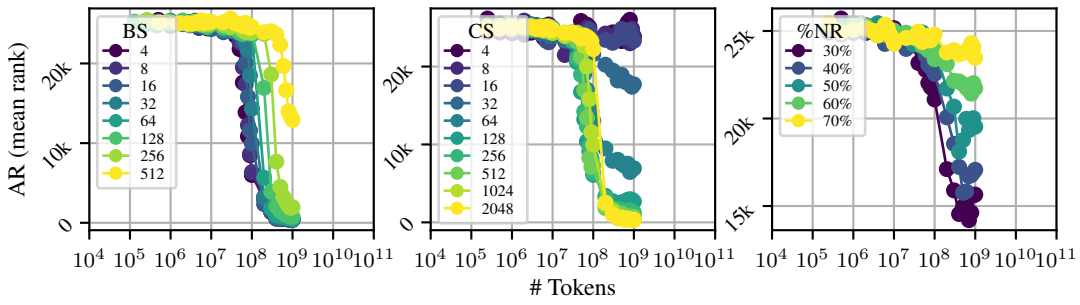


Figure 11. Developmental trajectories of AR (mean rank) of LMs with various batch sizes (left), context sizes (center), and repetitions (right) over the course of 1B tokens of pretraining, plotted against the number of updates (a) and the number of tokens (b). BS, CS, %NR stands for batch size, context size, and the proportion of chunks with no repetitions, respectively.

## J.2. Experiment 2

We replicate the analyses from Section 6 with LA in Figure 12b, AR (accuracy) in Figure 13a, and AR (mean rank) in Figure 13b. Overall, the Pareto frontiers found in these results are consistent across different metrics. For example, PS and LA seem to draw the same line between the configurations where IHs emerge and those where IHs do not emerge. However, it is important to note that, while the bottom right region,  $\in \{P(A, B, \dots, A) > 0.1 \cap P(A, B, \dots, A, B) > 0.5\}$ , is filled with highly strong IHs (as indicated by bright yellow) for PS, it is not the case for LA. In particular, the bottom right configuration,  $P(A, B, \dots, A) = P(A, B, \dots, A, B) = 0.9$ , results in a moderate IH, weaker than other configurations with less repetitions.

AR (accuracy), on the other hand, seems not to show a line as clear as the other three metrics. While the no-IH region seems to be very similar, IH-regions near the Pareto frontier in PS and LA are more graded for AR (accuracy). This indicates that even with the emergence of strong IHs high in both PS and LA, AR accuracy can still be low. This again highlights the sequential nature of the emergence of latent and surface capabilities (Reddy, 2024).

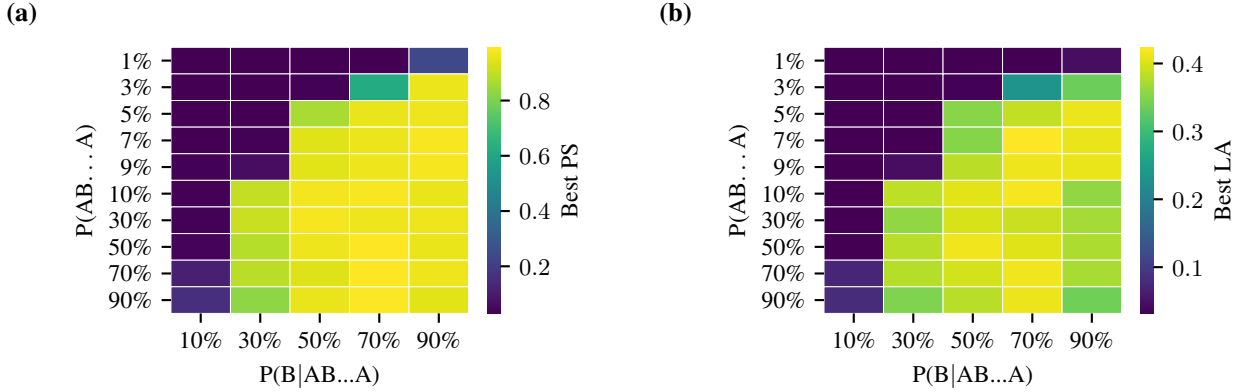


Figure 12. Best PS (a) and best LA (b) across all heads at the end of the training for each frequency reliability combination. Scores are represented in colors, with brighter colors representing higher scores.

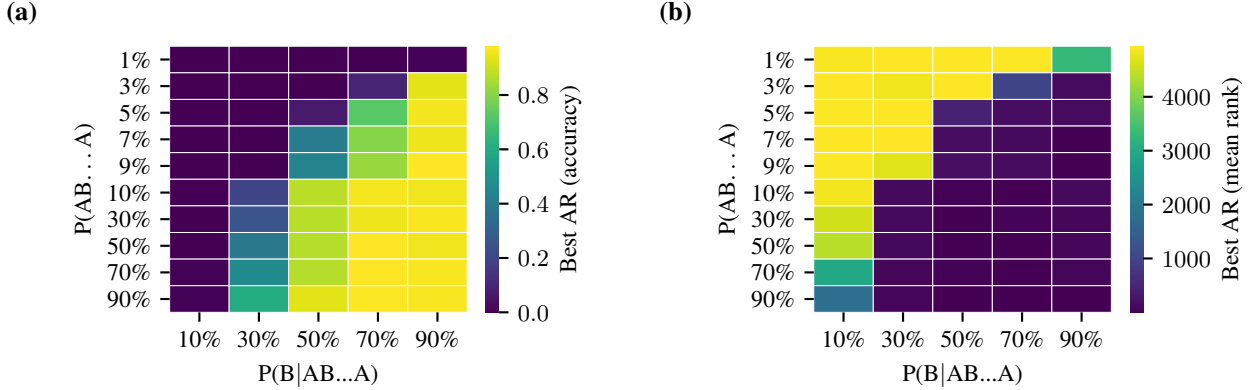


Figure 13. AR accuracy (a) and AR mean rank (b) at the end of the training for each frequency reliability combination. Scores are represented in colors, with brighter colors representing higher scores.

### J.3. Experiment 3

We showed in Section 7 that, when measured by PS, IHs form when the underlying distribution of the data generation process is  $+D$  and high in both repetition frequency and reliability (0.9-0.9) regardless of the distribution shape, and when it is  $+D+C$  and Zipfian when the repetition frequency and reliability is near the Pareto frontier (0.1-0.3). Here, we replicate the same analyses in LA (Figure 14b), AR (accuracy; Figure 15a), and AR (mean rank; Figure 15b). We make two observations. First, in each metric, Zipf $_{[+D+C]}$  is consistently the only distribution shape that promotes the emergence of IHs when the bigram repetition is near the Pareto frontier (0.1-0.3).

Second, and more importantly, contrary to the observation we made in Section 7, IHs do form even when the underlying distribution is  $-D$ , meaning that each token is i.i.d. However, it is important to note that the training data sample generated from this distribution is highly unlikely to be  $-D$  nor is each token in the training data i.i.d., given the constrained generation process described in Appendix G. Because we impose  $P(A, B, \dots, A)$  and  $P(A, B, \dots, A, B)$  while sampling from the generation, each sample is not independent of each other, violating the  $-D$  constraint. However, the reason why these training data sampled from underlying distributions  $^*_{[-D-C]}$  with high bigram repetition (0.9-0.9) leads to a low score in PS (Figure 5) but high scores in other metrics (Figures 14b, 15a and 15b), remains unclear, and warrants further investigation. Generally, studying these heads low in PS but high in LA could potentially reveal an alternative mechanism for IHs.

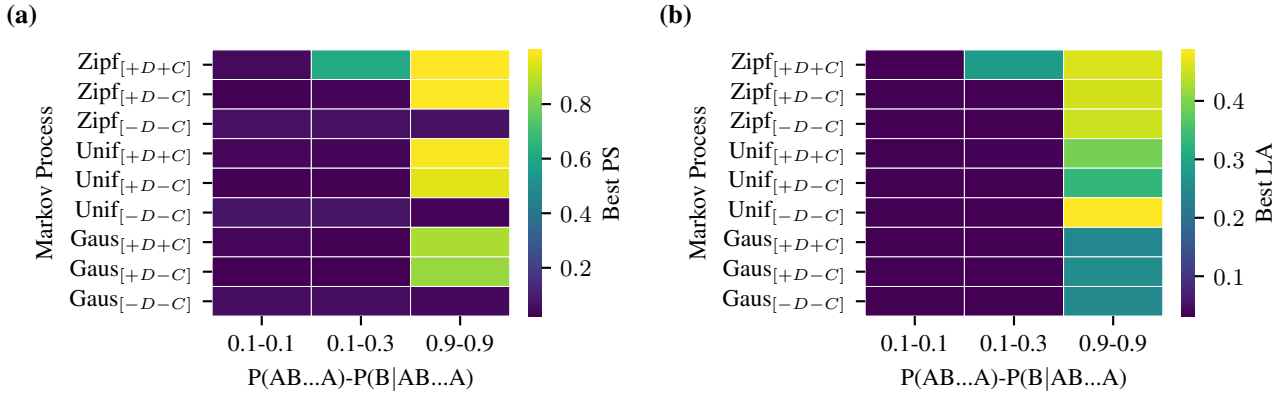


Figure 14. Best PS (a) and best LA (b) at the end of the training for each frequency reliability combination. Scores are represented in colors, with brighter colors representing higher scores.

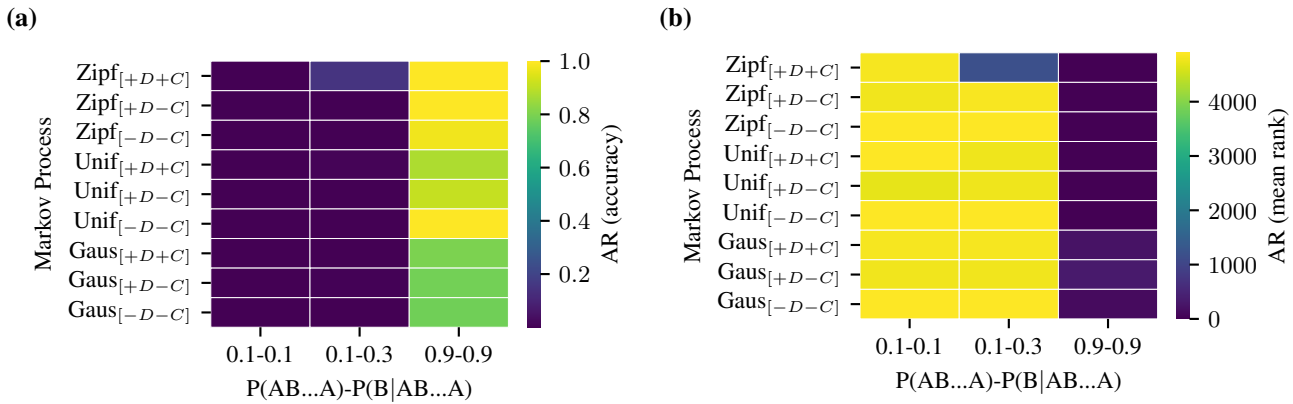


Figure 15. AR accuracy (a) and AR mean rank (b) at the end of the training for each frequency reliability combination. Scores are represented in colors, with brighter colors representing higher scores.